Acta Cryst. (1988). A**44**, 905-912

A Practical Direct-Space Refinement Cycle for Structure Images

BY P. GOODMAN

School of Physics, University of Melbourne, Parkville, Australia 3052

S. C. RAE

Department of Physics, Monash University, Clayton, Australia 3168

AND P. A. TULLOCH

Division of Protein Chemistry, Parkville, Australia 3052

(*Received* 3 *December* 1987; *accepted* 16 *May* 1988)

Abstract

A direct-space refinement method is described based on the procedure of placing a digitized electron-microscope unit-cell image in the frame store of an image-simulation computer to permit an iterative calculation. The material under investigation is $Rb_{22-5x}Nb_{54+x}O_{146}$, previously refined by X-ray single-crystal diffraction, which has tunnels with non-stoichiometric ionic occupation. It is concluded from this study that for problems where the major part of the structure is known the weak-phase-object approximation is adequate for the inversion component of a refinement provided only the x, y coordinates of the missing ions are required. An improved procedure which could allow refinement of the interatomic potential is suggested, incorporating the assumption that the structure consists of spherical atoms.

1. Introduction

It is now almost universally accepted that high-resolution lattice images require matching with an N-beam simulated image before a structural interpretation can be made. It is this acceptance that has allowed high-resolution images of inorganic oxides to be interpreted in terms of the structure instead of just the lattice, and has led to the term 'structure imaging' replacing that of 'lattice imaging' when the right conditions are met (Cowley, 1981, ch. 13). It is in principle impossible to invert the image-simulation process and drive the experimental image consisting of the intensity distribution $\psi\psi^*$, resulting from an N-beam-dynamic scattering process, back to a model structure. Approximate inversion procedures do exist, however, for very thin periodic and aperiodic structures, where it might be assumed that the kinematic or thin-phase-grating (Cowley & Moodie, 1959) approximations are valid. These are the 'weak-phase-object approximation' (Cowley, 1981), the 'projected-charge-density approximation' (Lynch, Moodie & O'Keefe, 1974), the 'thick-phase-object approximation' (Cowley & Moodie, 1962) and the 'pseudo-weak-phase-object approximation' (Li, 1987; Li & Tang, 1985). The first two of the above have been used in light-atom-organic-structure image interpretation (Grinton & Cowley, 1971) and for interpretation of unit-cell-size surface step structures (Lynch *et al.*, 1974), respectively.

In the commonly occurring situation where a structure is under study by both single-crystal X-ray diffraction and high-resolution electron microscopy, it is very likely that the average structure will be derived from the X-ray data, possibly over-symmetrized because of the limitations imposed by Friedel's law, and that the local and aperiodic structure will be solved by the microscope study. This procedure dates back to the beginning of structure imaging, from Allpress, Hewatt, Moodie & Sanders (1972) with respect to aperiodicity, and Cowley & Iijima (1972) with respect to the real-space-symmetry observation. Acceptance of the above developments leads to the possibility of digitization of the above process, and hence of a refinement cycle, since a difference, $\Delta I = I_{obs} - I_{calc}$, if small, may be invertible in some approximation. Under these circumstances, a refinement procedure can be constructed with some parallels to the difference-synthesis refinement methods of X-ray diffraction, but in direct space rather than reciprocal space.

In this paper we present results in which the above procedure is used to determine the x, y coordinates of ions in the non-stoichiometric tunnel structure $Rb_{22-5x}Nb_{54+x}O_{146}$.

2. Earlier study

The $Rb_{22-5x}Nb_{54+x}O_{146}$ structure has been the subject of previous high-resolution electron-microscope studies (Olsen, Goodman & McLean, 1983; Goodman, McLean, Wilson & Olsen, 1984). From these it is known that the symmetry of the local structure is

0108-7673/88/060905-08$03.00

$P2_1$, although the average symmetry as determined by convergent-beam electron diffraction (Goodman, 1984) is tetragonal, with the space group $P4/mbm$, consistent with the symmetry of the framework structure as originally determined by Gatehouse, Lloyd & Mishkin (1972). Further refinement of the structure from the electron-microscope images has proved impossible until now since insufficient data on the location of the tunnel ions are available and, especially in the case of the large septagonal tunnels, there are no known rules for making an intelligent guess. For singly occupied octahedral sites there exist Megaw's rules (Megaw, 1973), but no equivalent rules are available for doubly occupied tunnels of different geometry.

Fig. 1 shows a diagrammatic representation of this tunnel structure, known as a GTB (Gatehouse tungsten bronze) structure type (Bhide & Gasperin, 1979). The framework structure, formed from NbO_6 octahedra (Fig. 1*a*) is negatively charged (Bhide & Gasperin, 1979), and the stable cation-filled structure (Fig. 1*b*) has both Rb and Nb ions in the tunnels. In order to achieve the stoichiometry $Rb_3Nb_{54}O_{146}$ and charge balance, which other evidence (Goodman *et al.*, 1984) indicates is achieved over several unit cells in the *xy* plane, these sites have only partial occupation in the idealized unit cell. This idealized structure (Fig. 1*b*) is the result of a single-crystal X-ray

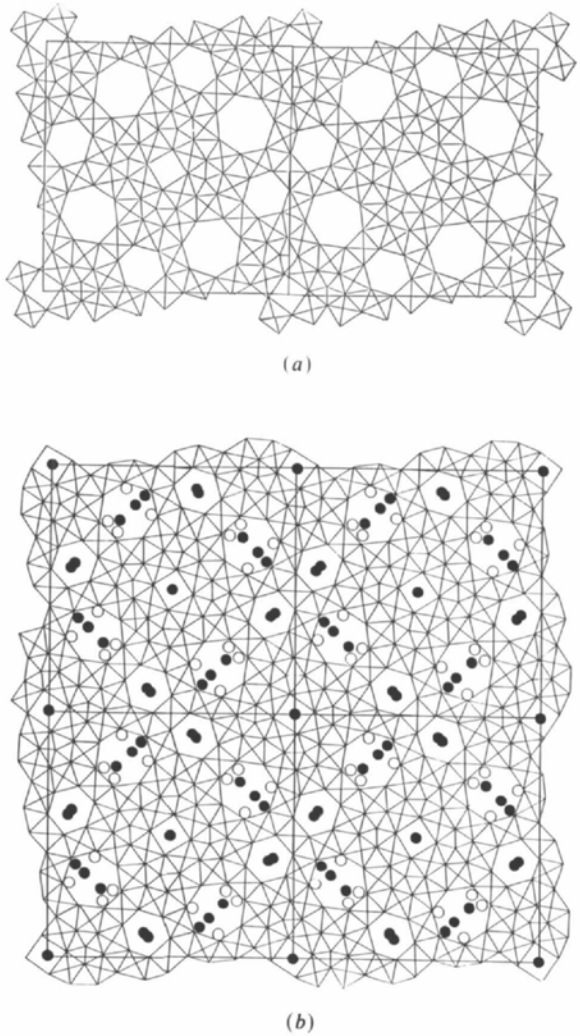

(*a*)

(*b*)

Fig. 1. (*a*) Schematic diagram showing two unit cells of the Nb_2O_5 framework structure projected along the *c* axis, as determined by Gatehouse and co-workers. (*b*) Structure of (*a*) with the tunnel ions – Rb (filled circles) and Nb (clear circles) – shown in the tunnels according to the single-crystal X-ray diffraction refinement carried out in the tetragonal system (four unit cells).

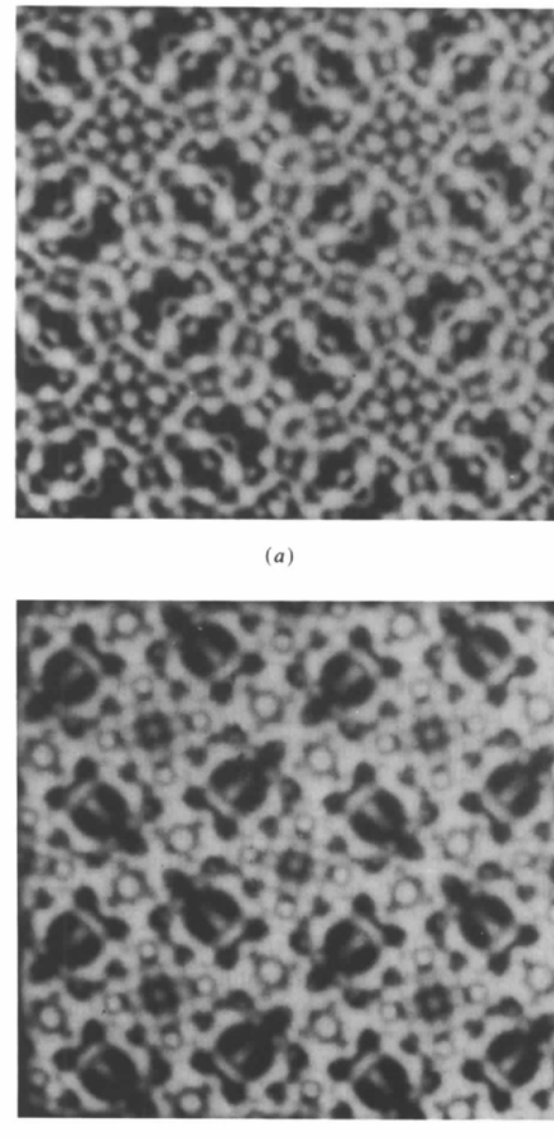

(*a*)

(*b*)

Fig. 2. Image simulations due to Olsen (1983) for the structure of Fig. 1(*b*), for crystal thickness 51·3 Å and defects of focus (*a*) −500 and (*b*) −800 Å and $R > 20 \times (d_{100})$.

refinement (Gatehouse, Goodman, Olsen & McLean, 1988) following Fallon & Gatehouse's (1980) procedure. Olsen (1983) earlier determined a full set of electron-microscope-image simulations for this idealized structure, and two frames from his simulation appear in Fig. 2. Unfortunately, these simulations, which have great asthetic appeal, bear no resemblance to the experimental results. The simulations contain no damping functions, apart from the use of isotropic room-temperature B factors, and of the 200CX transmission function determined by Glanville, Moodie, Whitfield & Wilson (1986). Given the complexity of the averaged structure, and the extreme sensitivity of the simulations to tunnel-ion location, this failure is hardly surprising since an X-ray-determined unit cell is likely to be both over-symmetrized and over-densely occupied.

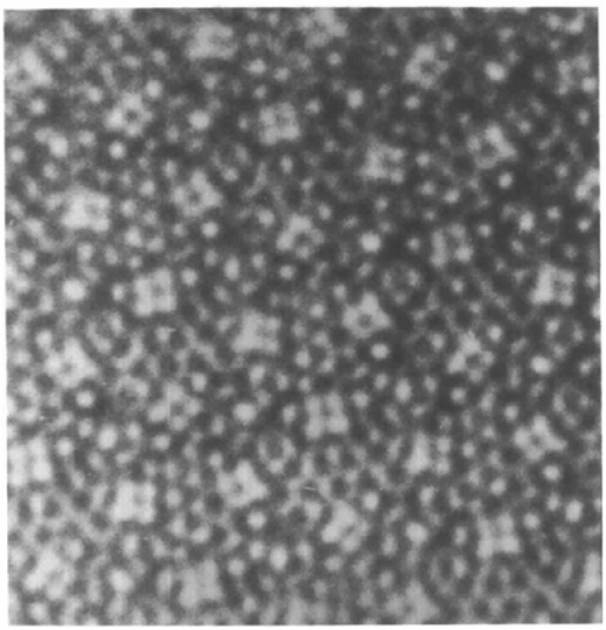

(*a*)

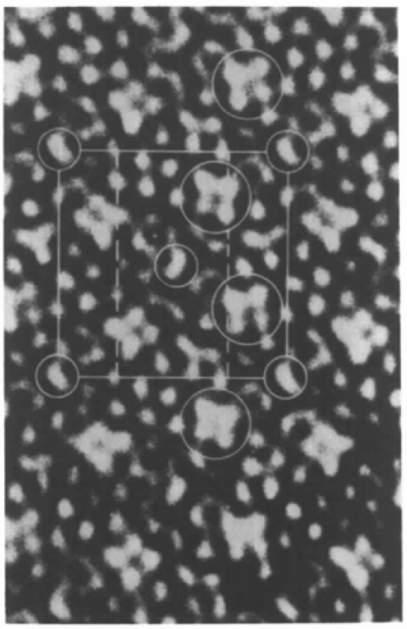

(*b*)

Fig. 3. (*a*) Image field from the $Rb_{22-x}Nb_{54+x}O_{146}$ preparation at the [001] zone axis. (*b*) Image segment with the space group *pg* drawn over the projected unit cell.

Fig. 3(*a*) shows the experimental image field taken down the 3·96 Å axis, the alignment being determined from the maximal local symmetry of $P2_1$ occurring in this compound, giving *pg* projection symmetry as shown in the segment of Fig. 3(*b*). These zone-axis micrographs show a typical four-pronged star image from the large tunnels and, across the square tunnel, which would be the site of a fourfold axis in $P4/mbm$ refinement, the image shapes are different and unrelated by symmetry.

The complexities of computer matching tunnel images increase with tunnel size. Thus the smallest square tunnel could be simulated with the structural assumptions of Fig. 1, and its occupation density estimated (Olsen *et al.*, 1983; Goodman *et al.*, 1984). The hexagonal tunnel images could be simulated with respect to their trigonal shape and central image densities, but not with respect to their orientation: the experimental alignment of the trigonal stars requires some departure from the ideal tetragonal framework of Fig. 1(*a*). The simulation of the largest septagonal tunnel was least successful since the experimental four-prong star could not be reproduced by trial-and-error selection of the sites of Fig. 1(*b*). These images clearly require more sophisticated analysis, and can only be understood by assuming some twofold occupancy within the crystal segments used, which are several unit cells thick.

3. Present procedure

For the refinement we started with the empty framework structure as determined by Gatehouse *et al.* (1972), and experimental images. The cycle used is shown in block diagrammatic form in Fig. 4. The weak-phase-object approximation (WPOA) was used as an expression in ΔV, as

$$\Delta V = (1 - \Delta I)/2\sigma,$$

where σ is the interaction constant. Before preparing the difference calculations, both the calculated and digitized data must be scaled to make the vacuum wave = 1.

Initially, a suitable micrograph was digitized with an Optronics Photoscan microdensitometer, using an identical framestore coordinate reference to that used in the image-simulation computer. Since the vacuum

is taken into the micrograph digitization, the resulting I_{obs} is on an absolute scale. Image simulation was performed on an Olivetti M24 IBM-compatible XT microcomputer, using software recently developed by Lynch & Qin (1987). This computer was linked to a Hewlett-Packard A900 minicomputer with high-resolution graphics display and half-tone hard-copy facilities.

4. Results

At first the instrumental parameters critical to the simulation, namely defect of focus Δf, spherical aberration coefficient C_s, diffraction aperture R (expressed in units of d_{100}, determining the number of beams used in the simulation), as well as the value of an isotropic temperature factor assumed for all atoms of the structure, B, were allowed to vary from their initial predetermined values, in separate trial computations. This allowed the operative values of these parameters to be determined by qualitative comparison of computed and experimental images. As a result the values $C_s = 0{\cdot}95$ mm, $\Delta f = -665$ Å, $R = 15 \times (d_{100})$ and $B = 2{\cdot}0$ Å^2 were arrived at, compared with the initial values of 0·95 mm, −650 Å, $20 \times (d_{100})$ and 2·0 Å^2 for the same parameters. Here the only significant change from the 'theoretical' values is the reduction in effective diffraction aperture from 20 to $15 \times (d_{100})$. The logic of this reduction may be stated in either of two ways: (*a*) that the aperture up to $R = 15$ contains the information relating to atomic and ionic positions being refined, while the region 15–20 contains the irrelevant details of an X-ray determined model; or (*b*) that images of single unit-cell area from thin crystal regions lack the sharp details implied by diffraction patterns obtained only from relatively large crystalline volumes. This point, concerning the degree of randomness present in single-cell images, is discussed further in § 5. The initial empty-tunnel simulated image obtained with these parameters is shown in Fig. 5(*a*) for a crystal thick-

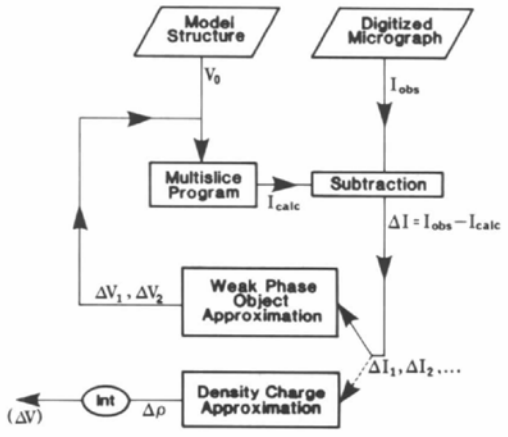

Fig. 4. Block diagram showing the refinement cycle used.

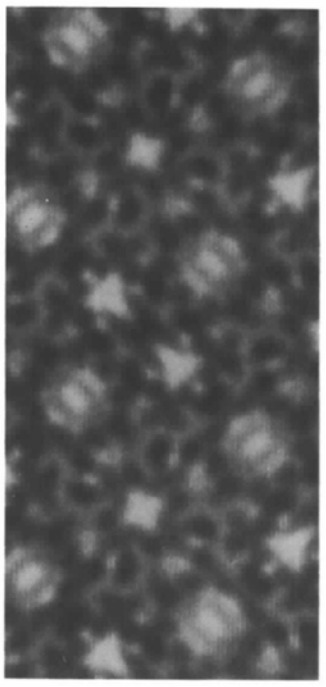

(*a*)

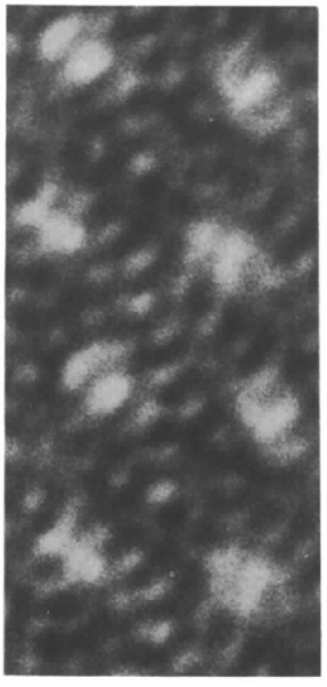

(*b*)

Fig. 5. (*a*) Simulated image for the framework structure, made with the microscope and crystal parameters: accelerating voltage = 200 kV, $C_s = 0{\cdot}95$ mm, $\Delta f = -665$ Å, $R = 15 \times (d_{100})$ and crystal thickness = 39·6 Å. (*b*) Experimental image field obtained from a crystal tilted a few milliradians from the exact zone axis.

ness of ten unit cells. Once the blackening curve for the emulsion and the above instrumental parameters have been established, the crystal thickness may be simply found from the subtraction $I_{obs} - I_{calc}$, when we restrict our choices to integral values of 3·96 Å. If too large or too small a thickness is chosen for I_{calc}, quite obvious very large negative or positive peaks appear in ΔI. For the area of micrograph digitized, ten unit cells thickness gave believable difference oscillations and identifiable shift functions for framework-Nb-atom sites.

The Fig. 5(*a*) simulation preserves the fourfold symmetry of the input together with a characteristic three-bar structure in the large-tunnel images. This structure is not seen in aligned experimental images, but has some similarity to detail appearing *without* fourfold symmetry, in off-axis images such as that shown in Fig. 5(*b*). This similarity suggests that for small tilts parallax obscures some of the tunnel-ion potential in projection.

We proceeded with the iteration, examining the projected potentials at the start (V_0) and after iteration. These potentials are shown in Figs. 6(*a*)-(*d*). After two iterations, peaks form in the tunnels, at sites marked in Fig. 6(*c*) only; Fig. 6(*d*) shows the same picture unmarked so as not to obscure the details. In addition to producing tunnel-ion peaks, the iteration modifies the framework structure, producing a distortion from the regular octahedra

Table 1. *Tunnel-ion coordinates derived from Fig.* 6

	x	*y*
Septagonal tunnel		
Rb 1	0·187	0·323
Rb 2	0·688	0·177
Nb 1	0·135	0·253
Nb 2	0·777	0·211
Square tunnel		
Rb	0·506	0·495
Hexagonal tunnel		
Rb	0·398	0·101

derived from a higher space group. Finally, some confidence for the resulting large-tunnel ion-peak coordinates can be gained from the fact that the ion positions found in the smaller tunnels correspond well with those estimated by trial-and-error image matching. The Rb- and Nb-ion coordinates for the three partially occupied tunnels of the asymmetric unit found in this way are given in Table 1. These coincide only roughly with selected sites determined by the refinement from X-ray data carried out in the *P*4/*mbm* space group (Gatehouse *et al.*, 1988) but the latter were used to distinguish Rb from Nb sites. Thus, Rb ions are more centrally located while Nb ions are located near the tunnel walls.

Fig. 7(*c*) shows the image detail, across the fourfold tunnel, which is the centre-of-symmetry site in the tetragonal model, simulated from V_1 (after the first iteration). This shows a distinct improvement over

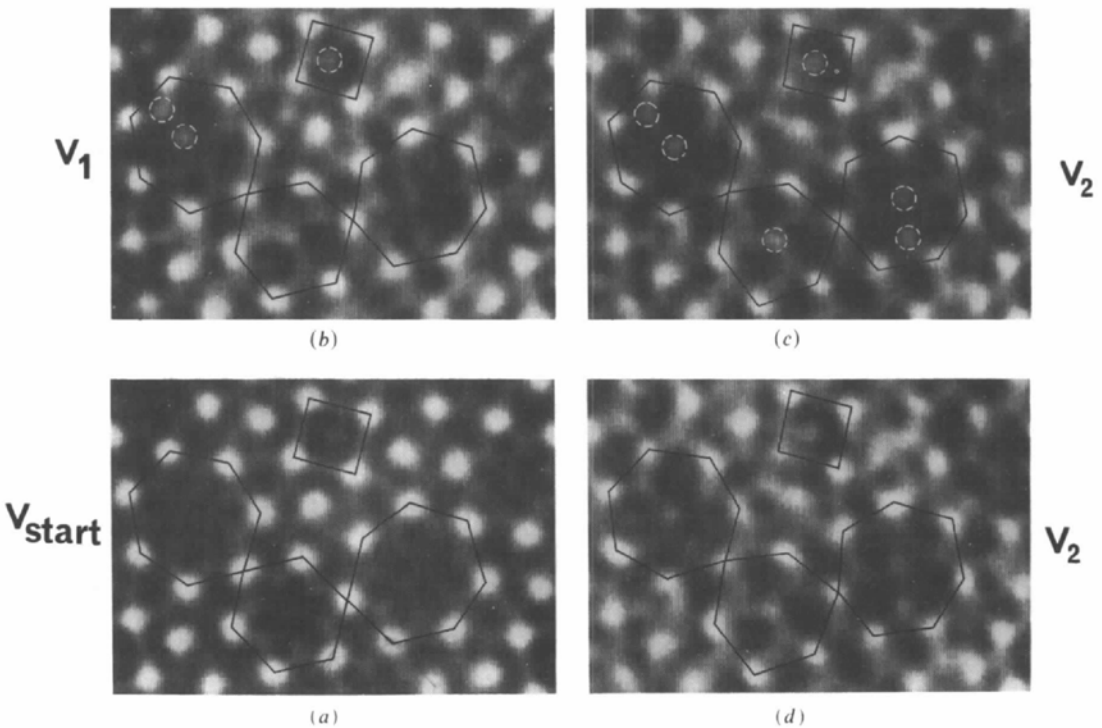

Fig. 6. Projected potentials obtained during the refinement cycle. (*a*) Initial potential V_0. (*b*) Result after one iteration. (*c*) Result after two iterations, with tunnel peaks encircled. (*d*) Same result as in (*c*) with sites unmarked.

the image simulated from V_0 in Fig. 7(b) with respect to the large-tunnel image detail, and the beginnings of a four-pronged tunnel image. This is an encouraging result from only one iteration, since we had previously failed to get any such character by trial and error. As an image match, however, the result leaves a lot to be desired (compare Figs. 7a and c), and further iteration by this primitive method produces no improvement, owing to the poor signal-to-noise content present in ΔI.

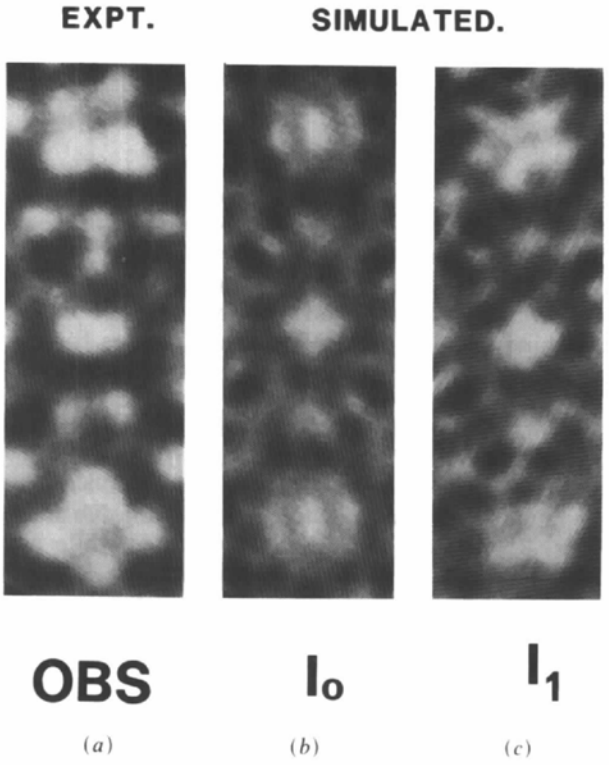

Fig. 7. Image sections across the square tunnel: (a) Experimental result. (b) Simulation from V_0 (initial potential). (c) Simulation from V_1 (first iteration).

5. Present limitations

Plots of ΔV obtained using the weak-phase-object approximation are shown in Figs. 8(a) and (b), after the first and second iteration, respectively. An inspection of these distributions shows that ΔV_1 contains both real information and termination noise in the approximate ratio 1:1, but in ΔV_2 almost no signal remains. The r.m.s. value of the ΔV distribution was 0·083 for ΔV_1 and 0·060 for ΔV_2; this reduces again slightly on additional iteration but not in a useful way. The origins of the termination noise are not difficult to find. Firstly, the weak-phase-object approximation contains no lens transfer function. Whilst it would have been possible to attempt some deconvolution procedure as recommended by Li (1987), it is quite valuable to see how much information can be derived from simpler inversions.

A second reason for the noise in the ΔV plots is the fact that simulated images made from a perfectly periodic model, at least with the present type of structure and specimen preparation, invariably contain more high-frequency detail than the experimental image. Visual inspection will usually show that neighbouring unit-cell images are not completely identical, so that if an average is struck from an area to eliminate noise high-frequency terms are inevitably cancelled.

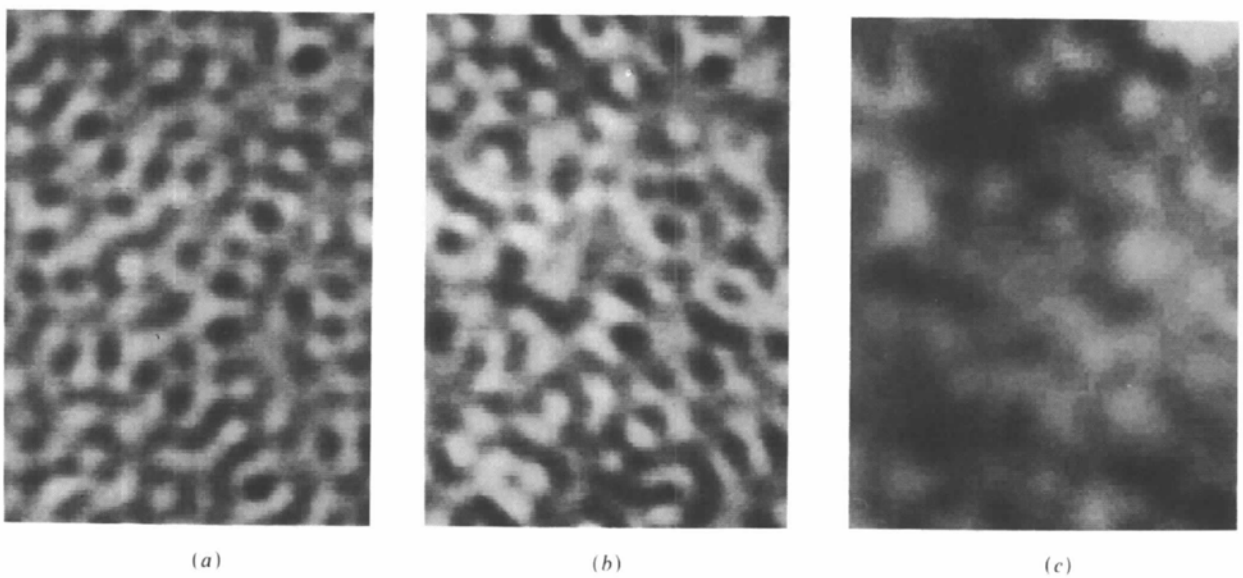

Fig. 8. Plots from ΔI resulting from the subtraction of Fig. 4, showing ΔV obtained using the weak-phase-object approximation from (a) the first and (b) the second iteration, respectively. (c) ΔV obtained after one iteration by assuming the projected charge-density approximation.

This fact is perhaps only made obvious when direct digital subtraction is employed. When a single unit-cell image is digitized, this still contains information from ten unit cells in projection and we are forming an average in depth. We can expect spatial variation in the micrographs to have at least three causes: (*a*) crystal surfaces formed by fracture may not be smooth, causing refractive variations; (*b*) there may be a real random variation in atomic coordinates between unit cells, which must be the case since tunnel-ion density is less than 1 per cell; (*c*) beam heating may cause higher than allowed for thermal vibrations.

Clearly we need to look at the next step to be taken in order to overcome the limitation encountered with the simple WPOA iteration. For the sake of comparison on this matter, the 'projected charge-density' approximation (PCDA) was tried, as a means for converting the distribution ΔI into a potential correction ΔV. In this case a Fourier-transform equivalence was used to invert Poisson's equation, so that

$$\Delta V \propto (\mathrm{FT})^{-1}[f(u)/(u^2+v^2)],$$

where $f(u)$ is the Fourier transform of ΔI, u and v are the reciprocal-space coordinates and $(\mathrm{FT})^{-1}$ represents the inverse Fourier transform. The resulting distribution, shown in Fig. 8(*c*), contains only low frequencies and demonstrates the inadequacy of the PCDA at the magnification of high-resolution imaging. At least the WPOA offers a chance to refine the structure at the atomic level, even though it lacks any of the damping offered by a lens function and consequently has an excessive amount of termination error.

From the present results then, a better approach is to retain the WPOA for initial iteration, but to send the refined potential back to an earlier stage in the cycle, *i.e.* to the initial atomic model as suggested in the block diagram of Fig. 9. This is equivalent to making use of the information that the structure is atomic, with spherical (circular) units in projection.

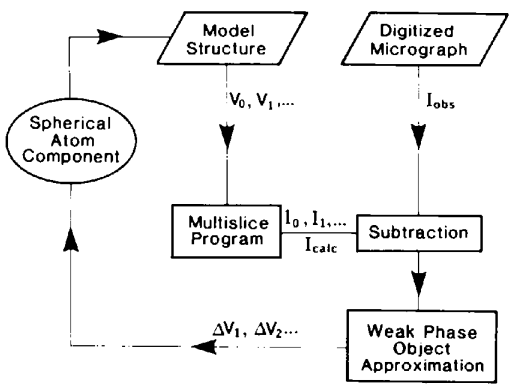

Fig. 9. Block diagram showing the suggested improved refinement cycle which takes account of atomization of the structure.

Since most of the iterated noise is non-spherical in character, such a step can only improve the refinement. Then, only at a late stage of refinement, when image match appears good, could any attempt to refine interatomic potential be considered.

6. Concluding remarks

The present example has shown that in some metal oxide studies the WPOA may usefully be incorporated in a computerized refinement cycle, provided the aim is restricted to refining the atomic coordinates of the projection. In the particular example chosen, failure of the trial-and-error method of refinement was due to an inadequate knowledge of the structure at the unit-cell level. The problem was not simply that of locating the tunnel sites, but also that of an unsuspected local distortion of the framework structure. This result emphasizes the value of employing a method incorporating a stage of image inversion to locate the main structural errors. An improved procedure suggested by this experience is one which would allow only the spherical-atom coordinates of the inverted difference to be retained in the cycle.

With the present improvements in electron-microscope-image recording systems, it is likely that any future work on digitized refinement will be done on directly recorded images from a video framestore rather than through the intermediate stage of digitizing photographs. Because of the additional power to check alignment and defocus, direct observation and recording is likely to increase greatly the application of the difference method.

References

ALLPRESS, J., HEWATT, E., MOODIE, A. F. & SANDERS, J. M. (1972). *Acta Cryst.* A**28**, 528-536.
BHIDE, V. & GASPERIN, M. (1979). *Acta Cryst.* B**35**, 1318-1321.
COWLEY, J. M. (1981). *Diffraction Physics*, p. 290. Amsterdam: North Holland.
COWLEY, J. M. & IIJIMA, S. (1972). *Z. Naturforsch. Teil A*, **27**, 445-451.
COWLEY, J. M. & MOODIE, A. F. (1959). *Acta Cryst.* **12**, 360-366.
COWLEY, J. M. & MOODIE, A. F. (1962). *J. Phys. Soc. Jpn*, **17**, Suppl. B**11**, 86-91.
FALLON, G. D. & GATEHOUSE, G. M. (1980). *J. Solid State Chem.* **34**, 193-198.
GATEHOUSE, B. M., GOODMAN, P., OLSEN, A. & MCLEAN, J. D. (1988). In preparation.
GATEHOUSE, B. M., LLOYD, D. J. & MISHKIN, B. K. (1972). *Proc. 5th. Mater. Res. Symp. Natl Bur. Stand. Spec. Publ. No.* 364. *Solid State Chemistry*, p. 15.
GLANVILLE, S. R., MOODIE, A. F., WHITFIELD, H. J. & WILSON, I. J. (1986). *Aust. J. Phys.* **39**, 71-92.
GOODMAN, P. (1984). *Acta Cryst.* A**40**, 635-642.
GOODMAN, P., MCLEAN, J. D., WILSON, I. J. & OLSEN, A. (1984). *Analytical Electron Microscopy*-1984, edited by D. B. WILLIAMS & D. C. JOY, pp. 130-134. San Francisco Press.
GRINTON, G. R. & COWLEY, J. M. (1971). *Optik (Stuttgart)*, **34**, 221-224.

LI, F. H. (1987). *Acta Cryst.* **A43**, C247.
LI, F. H. & TANG, D. (1985). *Acta Cryst.* **A41**, 376-382.
LYNCH, D. F., MOODIE, A. F. & O'KEEFE, M. A. (1974). *Abstr. 8th Int. Congr. Electron Microsc. Electron Microscopy* 1974, edited by J. M. SANDERS & D. J. GOODCHILD, pp. 222-223. Canberra: Australian Academy of Science.
LYNCH, D. F. & QIN, L. C. (1987). *J. Appl. Cryst.* **20**, 442-444.
MEGAW, H. D. (1973). *Crystal Structures: a Working Approach*, p. 286. Philadelphia, PA: W. B. Saunders.
OLSEN, A. (1983). *Collected Abstracts. 14th Meet. Soc. Crystallogr. Aust., Morpeth, Australia.* The Society of Crystallographers in Australia.
OLSEN, A., GOODMAN, P. & MCLEAN, D. J. (1983). *Proc. 41st Meet. EMSA*, edited by G. W. BAILEY, pp. 40-41. San Francisco Press.

Acta Cryst. (1988). A**44**, 912-927

Visibility of Single Heavy Atoms on Thin Crystalline Silicon in Simulated Annular Dark-Field STEM Images

BY RUSSELL F. LOANE, EARL J. KIRKLAND AND JOHN SILCOX

School of Applied and Engineering Physics, Cornell University, Ithaca, NY 14853, *USA*

(*Received* 30 *November* 1987; *accepted* 25 *May* 1988)

Abstract

The multislice method, pioneered by Cowley and Moodie, has recently been adapted to simulate annular dark-field scanning transmission electron-microscope (ADF STEM) images. This paper presents a series of calculations using this new approach with experimental parameters appropriate for a VG-HB501 STEM to investigate the visibility of single heavy adatoms on thin crystalline silicon membranes. The tendency for electrons to channel along columns of atoms in crystals can greatly increase the intensity incident on an adatom on the exit surface, thereby increasing the adatom visibility. The simulations indicate that an adatom on the exit surface on a column of crystal atoms is up to three times as visible as an adatom on the entrance surface, and that the adatom remains highly visible as the crystal thickness is increased. Tilting the specimen or displacing the adatom from the column appears to lower the visibility of the adatom dramatically. These calculations suggest that, with the appropriate imaging conditions, a single gold adatom may be visible on at least 235 Å of (111) silicon.

1. Introduction

Images of single heavy atoms on very thin amorphous substrates were first produced using annular dark-field scanning transmission electron microscopy (ADF STEM) imaging techniques (Crewe, Langmore & Isaacson, 1975; Isaacson, Langmore, Parker, Kopf & Utlaut, 1976). In this situation, incoherent imaging conditions apply (Cowley, 1976), and a simple physical model in which the intensity scattered from each atom is added together linearly provides a description of the conditions for visibility of the heavy adatom. On crystalline substrates, diffraction can be a significant factor in the ADF signal (Cowley, 1973) and experimental images may be difficult to interpret (Donald & Craven, 1979). This difficulty has led to efforts to minimize dynamical diffraction effects by increasing the inner angle of the detector (Howie, 1979; Treacy, 1981) or by orienting the crystal away from the strong Bragg reflections found at low-order zone axes (Pennycook, Berger & Culbertson, 1986). As yet no experimental observations of single heavy atoms on crystalline substrates with ADF STEM have been reported, though the sensitivities produced to date suggest that one bismuth atom might have a 50% contrast in 270 Å thick silicon (110) crystals (Pennycook *et al.*, 1986).

An advantage of including diffraction in low-order axis imaging is that it may be possible to image the adatom and the crystal simultaneously, allowing the determination of the adatom position with respect to the crystal lattice. The difficulty is the image interpretation. As mentioned above, the response has been to set up experimental conditions to simplify this step, by discarding all crystal-lattice information. An alternative approach is to simulate the images and use the simulations as a guide to interpretation. This latter approach is now standard in conventional transmission electron microscopy (CTEM), and has been followed in this paper for STEM. A series of ADF STEM image simulations of heavy adatoms on thin crystalline silicon (111) films are presented as a guide to possible experimental studies.

Simulations are an essential tool of electron microscopy. Because image formation for crystalline specimens is a complex nonlinear process, simple analytical descriptions are inadequate. Interference effects can lead to significant misinterpretation of results (Engel, Wiggins & Woodruff, 1974). Numerically intensive simulations are necessary as a guide to the

0108-7673/88/060912-16$03.00